# Vertically-aligned short E-glass fibre core sandwich composite: Production and evaluation

White, Robbie; Machavaram, Venkata R; Fernando, Benjamin A; Paget, Mark A; Prasad, Ashwini; Fernando, Gerard F

*DOI:*
10.1177/1099636221993883



*Document Version*
Publisher's PDF, also known as Version of record

*Citation for published version (Harvard):*
White, R, Machavaram, VR, Fernando, BA, Paget, MA, Prasad, A & Fernando, GF 2021, 'Vertically-aligned short E-glass fibre core sandwich composite: Production and evaluation', *Journal of Sandwich Structures and Materials*, vol. 24, no. 1, pp. 109963622199388. https://doi.org/10.1177/1099636221993883

JOURNAL OF SANDWICH STRUCTURES & MATERIALS

*Original Article*

*Journal of Sandwich Structures and Materials*
0(0) 1–27

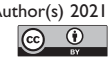
Article reuse guidelines:
sagepub.com/journals-permissions
DOI: 10.1177/1099636221993883
journals.sagepub.com/home/jsm
SAGE

# Vertically-aligned short E-glass fibre core sandwich composite: Production and evaluation

**Robbie White, Venkata R Machavaram, Benjamin A Fernando, Mark A Paget, Ashwini Prasad and Gerard F Fernando**

## Abstract

This paper reports on the production and evaluation of a new class of "Z-axis" composite sandwich panel where the core consists of a dense array of vertically-aligned, 3 mm long E-glass fibre composite "beams". The E-glass fibre bundles were aligned using electrostatic charging. A procedure was developed to retain the orientation of the short-fibre bundles whilst they were impregnated and cured with an epoxy/amine resin system. The skins were manufactured from 4-ply carbon/epoxy prepregs with a layup sequence of $(0,90)_s$. The out-of-plane compressive strength of these Z-axis composites was found to be 25.2 and 15.2 times greater than equivalent sandwich panels made with Nomex® and aluminium honeycomb cores respectively. Their compressive strength was found to increase in proportion to the density of the core. Buckling and fracture of the vertically-aligned Z-axis composite were the predominant failure modes observed. The shear and flexural properties of the Z-axis composites were comparable to equivalent honeycomb sandwich panels manufactured from Nomex® and aluminium honeycomb cores.

## Keywords

Sandwich composite, honeycomb, vertically-aligned, impregnation, flatwise compression

Sensors and Composites Group, School of Metallurgy and Materials, University of Birmingham, Birmingham, UK

**Corresponding author:**
Gerard F Fernando, Sensors and Composites Group, School of Metallurgy and Materials, University of Birmingham, Birmingham, UK.
Email: g.fernando@bham.ac.uk

## Introduction

A sandwich composite panel consists of a lightweight core bonded to two stiff and strong reinforced outer skins. The skins are responsible for resisting the in-plane and bending loads whilst the function of the core is to resist out-of-plane compressive and shear loads. In applications where the sandwich panel is subjected to hydrostatic or compressive loading, the properties in the through-thickness or "Z-direction" are important [1]. A schematic illustration of selected designs of cores is shown in Figure 1.

Common materials that are used as the core include hexagonal honeycomb structures made from aluminium or Nomex® [2] as they offer high specific shear stiffness and strength [3]. The honeycomb structure provides a continuous path for shear loads to be transferred throughout the core. Polymeric and metallic foams are also used as the core in sandwich structures. Polymer-based foams tend to have a lower density than the honeycomb structures and offer excellent energy absorption characteristics. However, their specific compressive strength and stiffness are typically lower than the honeycomb structures [4]. Reinforcing fibres have been used as an alternative to honeycomb and foam-based cores. One such example is the "X-core" sandwich panel where elongated Z-pins were inserted through both skins prior to cross-linking the resin [5]. Cores have been manufactured consisting of Z-pins or combined with a foam where the X-core/foam panels are slightly heavier but exhibit better compressive properties [6]. The compressive properties were observed to be a function of the volume fraction and orientation of the Z-pins [5,7].

Stitching has also been used to introduce through-thickness reinforcement in preforms prior to impregnation and cross-linking of the matrix [8]. In a more recent development, the stitching process was modified to form a sandwich panel core consisting of composite columns [9]. The compressive strength was observed to increase linearly with the density of the stitched column. The stitching technique has also been adapted for the production of sandwich panels. For example, corrugated glass fabrics were stitched to the face-sheets [10–12]. Trusses have been used to form the core [13] and they have been reported to have similar

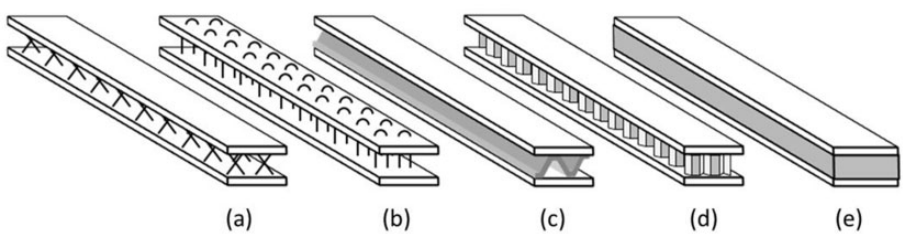


**Figure 1.** Schematic illustration of selected sandwich composites with specific core designs. (a) X-core Z-pinned core. (b) Stitched core. (c) Truss core. (d) Honeycomb core. (e) Foam core. Items (a) and (b) are sometimes used with a foam core.

compressive strength, for a specified density, when compared to aluminium and Nomex® honeycombs [3,14].

Other examples of innovation in the design of sandwich cores include shear-keying [15], tube-reinforced foam [16], composite rods [17], polymer/resin pins [18–20] and hybrid divided cores [21].

The current paper reports on a method to manufacture a new class of sandwich composite where the core consists of a dense array of vertically-aligned 3 mm long E-glass fibre bundles. The alignment of the E-glass was achieved using electrostatics and this class of sandwich design was termed "Z-axis composite". Details of the experimental methods that were used to manufacture the Z-axis preform are described along with the procedures that were used to bond and impregnate the vertically-aligned short-fibres. The flatwise compression, flexural and transverse shear properties were evaluated and compared with sandwich composites manufactured using equivalent Nomex® and aluminium honeycomb cores. A brief description of the theory for the electrostatic-based levitation of short E-glass fibres is presented. The flatwise compressive strength of these Z-axis composites was found to be approximately twenty-five and fifteen times greater than equivalent sandwich composite panels made using Nomex® and aluminium honeycomb cores respectively.

## Experimental

### Materials

***Selection criteria:*** The reinforcements and resins used in this study are readily available commercially. Furthermore, the short-E-glass fibres, carbon fibre skins and the primary resin that was used for impregnating the short-fibres are used extensively for manufacturing fibre reinforced composites. Cross-ply carbon fibre skins, in an epoxy/amine resin system, was selected for manufacturing the conventional honeycomb sandwich and the Z-axis composites; this was done to enable a direct comparison between the different classes of core materials. Short-E-glass fibre bundles are available commercially in lengths of 3, 3.2, 3.8 and 4.5 mm and they are mainly used for injection and compression moulding. 3 mm long E-glass fibre was chosen for the current study because the initial fundamental studies on the charging, fibre orientation upon deposition and charge-retention was carried out using these fibres [22,23].

The resin systems selected had to fulfil a number of criteria. In the first instance, it was necessary for the vertically-aligned short-fibre preform (on an adhesive-backed cellulose paper) to be bonded to the composite skin. The selection criteria for this resin system was that it needed to enable the spatial orientation of the vertically-aligned fibres to be secured to the skin relatively rapidly. The other options considered were: (a) photo-curable resins; (b) conventional resin films that are used to bond honeycombs to composite skins; (c) the primary resin system that was used to impregnate the short-fibre preform; and (d)

rapid-curing thermosetting resin systems. The two resin systems that were selected were Araldite-Rapid and Scotch-Weld 9323 where their pot-lives are approximately 5 and 120 minutes respectively. Both these resins are in the form of a relatively high-viscosity paste and hence, the probability of them wicking down the short-fibres was remote. The wicking of the resin will not be an issue if the same resin system, as that used to secure the vertically-aligned fibres, is also used to impregnate the short-fibre preforms. Araldite-Rapid was convenient because of its relatively short pot-life and rheological properties. Scotch-Weld 9329 was used to demonstrate that: (a) the Z-axis composite could be manufactured using high-performance structural adhesive with a relatively long pot-life; and (b) the mechanical properties of the sandwich composite could be optimised by the choice of adhesive. The primary resin system that was used for impregnating the vertically-aligned short-fibre preform was LY3505/XB3403. This resin was used as it has been characterised extensively by the authors previously with regard to its thermo-mechanical and spectral properties [24], impregnation characteristics [25], susceptibility to moisture ingress [26] and its cross-linking behaviour [27].

***Carbon fibre composite skins:*** The material used for the skins was unidirectional carbon fibre prepregs (VTM 264, T700, ACG, UK). The prepreg was sectioned and laminated to produce a 4-ply laminated preforms with a $(0,90)_s$ stacking sequence. The stacked prepreg was vacuum-bagged and processed in an autoclave using the cross-linking schedule recommended by the supplier [28]. The composite was sectioned to the required dimensions to prepare specimens for flatwise compression, flexural and transverse shear tests.

***Short-E-glass fibre bundles:*** 3 mm long E-glass bundles, ChopVantage® HP3540 fibres (PPG Industries, UK) were used as the Z-axis reinforcement [29]. The fibres were initially dried at 80°C for six hours and then stored in an air-tight container. Just prior to use, the fibres were dried at 60°C for two hours.

## Sandwich panels

***Conventional sandwich panels:*** The honeycomb cores were made from aerospace grade Nomex® (ANC-3.2-48) and aluminium (4.5-1/8-5052) and these were supplied by TenCate. The cell sizes in each case were 3.2 mm.

In the first series of experiments, Araldite-Rapid, a 2-part resin (Huntsman Advanced Materials, UK), was used for bonding the Z-axis preforms and the honeycombs to the carbon fibre composite skins. In subsequent experiments, the Z-axis preforms and the honeycomb were bonded using a high-performance adhesive (Scotch-Weld 9323, 3M, UK) [30].

The same epoxy/amine resin system, (LY3403/XB3503, Huntsman Materials, UK), was used to impregnate the array of vertically aligned short-E-glass fibre bundles [31].

***Production of Z-axis preforms:*** A schematic illustration of the electrostatic rig that was used to align the short-E-glass fibres is shown in Figure 2. The rig was enclosed in a Perspex™ chamber to restrict access when it was operational. The rig

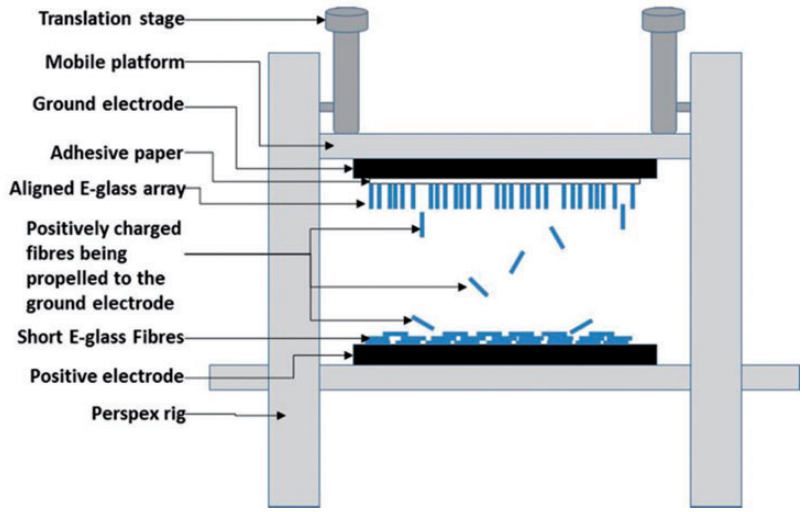


**Figure 2.** Schematic illustration of the electrostatic rig for producing the Z-axis E-glass fibre preforms.

consists of two 10 x 10 cm copper electrodes that were mounted on a Perspex™ sheet with the electrodes facing each other. The distance between the electrodes was adjustable via a pair of translation stages. The bottom and top electrodes were connected to the positive and electrically ground terminals of a high-voltage power supply respectively. A cellulose-based paper with an adhesive layer on one side was attached to the top electrode with the adhesive layer facing the bottom electrode; the attachment was achieved using masking tape thus enabling it to be demounted with ease. The rig was designed such that the positive and grounded terminals on the electrodes could be demounted to enable the weight of short-fibres that were deposited on the grounded top-electrode to be determined periodically. Approximately 10 g of the pre-dried short-E-glass fibres was spread evenly over the bottom electrode and the positive electrical terminal was attached to the power supply. The top electrode was attached to the ground terminal of the power supply. The distance between the electrodes was 22 mm and the applied potential was 9 kV. These parameters were chosen after a study to determine the processing parameters to enable the deposition of the vertically-aligned fibres on the grounded electrode without causing any significant chaining or discharging. Chaining of the fibres was avoided by charging the fibres in a cycling manner. Discharging between the electrodes was not prevalent at an electrode separation of 22 mm and the environmental conditions within the safety enclosure [22,23]. Under the applied field, the E-glass bundles become positively charged and are attracted to the top electrode, where they are adhered to the adhesive layer.

The electrical potential was applied in cycles of 4 minutes, with a dwell period of two minutes without the applied voltage. This allowed the charge on the

short-fibres to dissipate between cycles. This procedure was observed to increase the number of short-fibres leaving the positive electrode when the electrical potential was reapplied. During production involving longer cycles, some chaining was observed where the fibres were linked together as opposed to being deposited on the adhesive layer. A ground-electrode was used to discharge the rig at the end of the dwell period and then an insulating rod was used to dislodge any fibre chains. This resulted in a dense layer of vertically-aligned short-fibres on the adhesive layer. The number of cycles used was dependant on the spatial density of short-fibres that was required for the core.

After the desired fibre volume fraction of the short-E-glass fibres was deposited on the adhesive-backed cellulose paper, it was demounted from the rig. In the first series of experiments, a thin layer of an epoxy/amine adhesive (Araldite-Rapid) was applied to a pre-abraded and de-greased surface of the 4-layer cross-ply carbon fibre composite skin. The free-ends of the vertically aligned short-fibre array on the cellulose paper was positioned carefully on the composite skin with the adhesive layer. A flat steel plate was placed on the top along with a 2 kg weight to apply a lateral force during the bonding operation. The adhesive was permitted to cross-link for thirty minutes at ambient temperature. Once the short-fibres were bonded to the carbon fibre composite skin, the cellulose paper was removed. Photographs showing the production of Z-axis composites are presented in Figure 3(a) to (d). An optical micrograph of a short-E-glass fibres is shown in Figure 3(e) where the chopped (as-manufactured) fibre-ends are seen to be near parallel.

***Impregnation of the Z-axis fibre array:*** In the first series of experiments, impregnation of the short-fibres on the carbon fibre skin was achieved by placing the array of fibre-ends in a tray that contained the pre-mixed epoxy/amine resin system (LY3505/XB3403) for approximately ninety seconds. The depth of the liquid was approximately 1 mm. The impregnation of the bundle was achieved via capillary action. The excess resin was removed and the resin system was permitted to gel at ambient temperature for 24-hours before the second skin was bonded as described previously. This Z-axis composite was post-cured at 80°C for 6 hours in an air-circulating oven.

***Production of shear test specimens:*** Six each of the Nomex® and aluminium honeycomb sandwich composites were manufactured in the same manner as described previously. However, in this instance the length and width was 100 x 50 mm respectively. Twelve Z-axis sandwich composites with the same dimensions were manufactured as described previously. Six of the samples were manufactured using Araldite-Rapid to bond the short-fibres to the carbon fibre composite skins. With the remaining samples, Scotch-Weld resin was used. The procedure for impregnating the short-fibre samples that bonded to the skin using the Scotch-Weld resin was different. In this instance, the skins were initially bonded to the Z-axis preforms and then post-cured. Three edges of the sandwich panel were sealed and secured vertically with the open edges on the top to form a moat. The LY3505/XB3403 resin system was introduced into the sandwich preform to

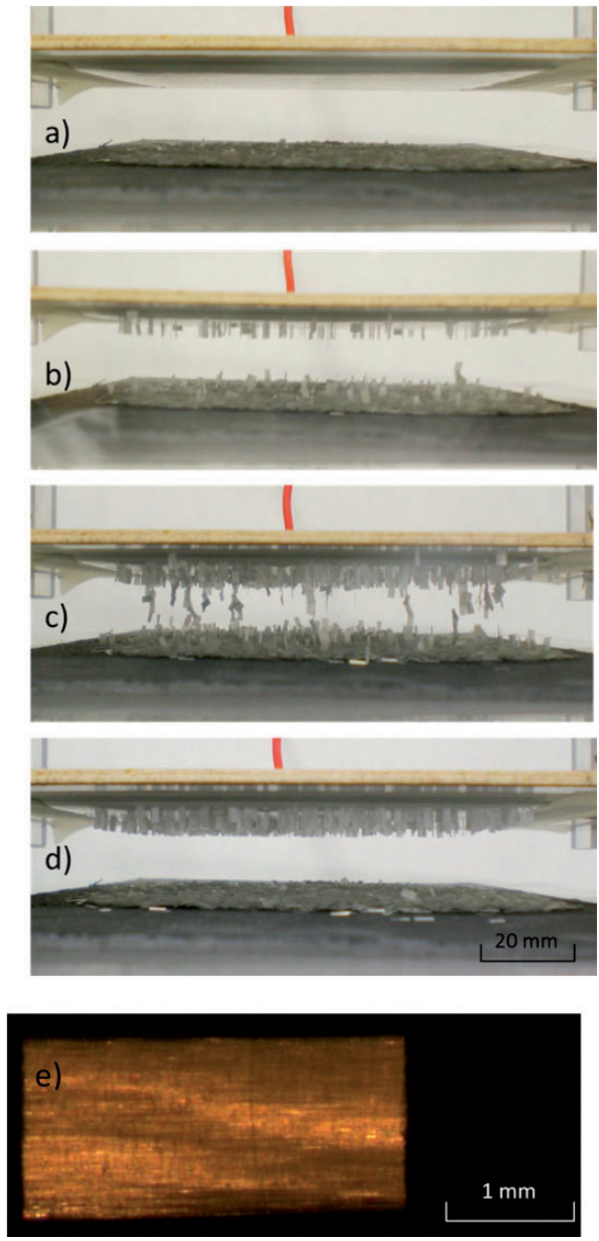


**Figure 3.** Photographs illustrating the production of the Z-axis preforms using an electrostatic field for deposition of the short-E-glass fibres. (a) A specified mass of pre-dried short-E-glass fibres is positioned on the positive electrode. (b) The application of an electrical potential results in the short-fibres being attracted to the grounded electrode. The adhesive paper retains the spatial orientation of the short-fibres on it. (c) Illustration of fibre chaining with prolonged application of the potential. (d) End of the production cycle where an array of vertically-aligned short-E-glass fibres are produced. (e) A magnified micrograph of a single short-E-glass fibre bundle.

impregnate the short-fibres. Once the cavity was filled, the moat was dismantled and the resin was permitted to drain out. A vacuum suction device was used to remove the excess resin. The sample was weighed periodically during the removal of the resin to ensure that the required resin content was achieved.

***Production of flexural test specimens:*** The Nomex®, aluminium and Z-axis sandwich composite panels were manufactured as described previously for the compression and shear test specimens. In order to comply with the specimen dimensions specified in ASTM Standard C393 [32], the width and length were 75 mm and 200 mm respectively.

### *Test methods*

***Flatwise compression:*** Flatwise compression tests were carried out in accordance with ASTM standard C365 [33]. An ESH servo-hydraulic uniaxial test machine with a load-cell capacity of 200 kN was used along with a cross-head displacement rate of 0.4 mm/minute. *In-situ* imaging of an edge of the sandwich panel was carried out using a Dino-lite Pro digital microscope camera.

***Shear Tests:*** Shear tests were conducted in accordance with ASTM standard C273 [34]. A plumb line was used to ensure the line of loading was in accordance with that specified in ASTM C273. The cross-head displacement rate was 0.4 mm/minute. As with the flatwise compression samples, the Dino-lite CCD camera was used to monitor the deformation characteristics of the core at the edge of sandwich composite during shear loading.

***Flexural stiffness and transverse shear rigidity:*** These properties were evaluated using three and four-point bending in accordance with ASTM standard D7250 [35]. The four-point bend tests were conducted first and terminated at a load of 500 N, where all the samples were observed to behave elastically up to this point. The samples were then tested past their yield point under three-point loading. A linear voltage displacement transducer was positioned directly below the mid-point of the sample to record the flexural deformation. The flexural tests were conducted at a cross-head displacement rate of 6 mm per minute. The flexural stiffness and the shear rigidity were calculated as specified in ASTM standard D7250 [35].

## Results and discussion

### *Levitation of short E-glass fibres using electrostatics*

A schematic illustration of the levitation of a short-E-glass fibre, under an applied electric field, is shown in Figure 4. The following section presents a brief description of the mechanism responsible for the levitation of the E-glass fibre. A summary of the relevant equations is also discussed.

E-glass is a dielectric material and its electrical conductivity and static dielectric constant are $10^{-14}$ S/m and 6.13 respectively [36]. The corresponding characteristic time-constant for charge dissipation, the ratio of permittivity to the conductivity, is

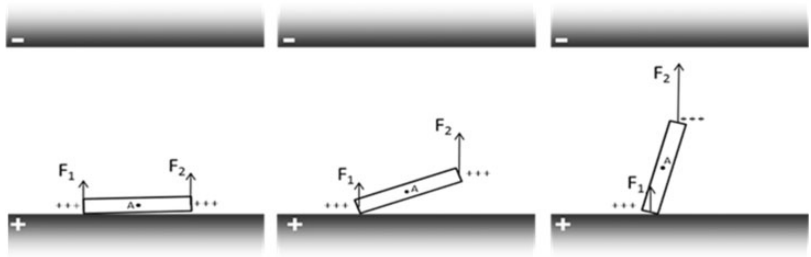


**Figure 4.** Schematic illustration of the electrostatic orientation of an E-glass fibre bundle. The accumulation of charge is non-uniform due to end-face topology of the chopped fibre-ends, the distribution of the binder within the bundle and its position (resting on other short-E-glass fibres – not shown). When an electric field is applied, the accumulation of charge is greater at one end and hence the magnitude of the force $F_2$ is greater than $F_1$. Hence, an initial orienting torque around point-A. The end of the fibre is lifted towards the grounded electrode.

36.78 x $10^4$ s. In general, the composition of the sizing and binder formulations used on the fibres are proprietary. The antistatic agents used in the binder are generally meant for dissipating the static free-charge on the bundle in a significantly shorter time [37]. In the current study, the higher conductivity of the binder due to the presence of antistatic agents, along with other additives, aids in the flow of charges from the positively charged bottom electrode to the short-E-glass fibre bundles. Polarisation-induced bound charge also appears on the dielectric E-glass fibres. The polarizability in a static DC field is proportional to the electric field strength and it is greater for materials with larger dielectric constant. However, the polarization-induced surface bound charge density ($\vec{P}.\hat{n}$) is immobile; $\hat{n}$ is the unit normal to the surface and P is the polarization of the E-glass [38]. The compositional homogeneity and thickness variations of the binder in between the filaments within the bundle, and over the surface, determines the entire volume and surface conductivities and hence, the charge distribution. The geometry of the E-glass fibre bundle resembles an array of parallel dielectric cylinders held together by a thinly coated binder medium with a significantly higher conductivity as compared to the E-glass fibres. When the continuous E-glass fibres are chopped, the topography of the cleaved-ends of the bundle is variable because: (a) the distribution of the binder is not constant; (b) the support rendered to the filaments in the bundle as they are sectioned; and (c) the profile and cross-section of the bundle will depend on its position along the length of the creel [39]. Therefore, it is reasonable to state that no two fibre bundles are identical topographically. The fibre chopping operation generates binder-free cleaved end-faces; hence their surface conductivity can be expected to be much smaller. Although the conductivity of the binder is much lower compared to that of the positively charged metal electrode, its finite conductivity enables the flow of charge from the plate to the entire surface of the E-glass bundles; the charge builds up with the applied potential until an equipotential steady-state is attained. The charge tends to flow towards the cut-edges of the

bundles in a similar fashion to that observed in metals. Such highly localised charge concentration at the cut-ends of the fibres is subject to strong electrostatic attraction via the uniform electric field in between the parallel plates of the capacitor rig. Prior to charging (see Figure 3), the E-glass fibres are spread manually over the positive electrode. However, not all the E-glass fibre bundles are in direct contact with the surface of the positively charged electrode (this is shown schematically in Figure 4). It is assumed that the conductivity of the binder aids in charging the bundles in spite of the fact that they are piled on top of each other. With reference to the experimental conditions mentioned previously and the prevailing laboratory conditions, it was observed that at an applied potential of 9 kV, owing to the variations in the charge concentration at chopped-ends of the fibre bundles, the torque generated eventually overcome the rotational inertia of the bundle. Hence, the bundle tends to align along the electric field and it levitates towards the grounded upper electrode as the electrostatic force exceeds the weight of the bundle (see Figures 3 and 4). The applied voltage required to levitate the dried bundles was found to have a variability of $\pm 1$ kV. Observations suggest that controlling the relative humidity, temperature and the atmosphere (air, inert gas, etc) can influence the electrostatic levitation of the short E-glass fibre bundles. The effect of humidity will be detailed in a subsequent publication.

The following section gives a mathematical interpretation of the electrostatic charging and the effect of forces on the fibre bundles.

***Charging dielectric fibres with a conductive coating:*** The polarization-induced and free-current densities contribute to the total current density $\vec{J}_T$ within the bundle. Hence, the continuity equation for the total current density can be represented as

$$\vec{J}_T = \vec{J}_b + \vec{J}_f \tag{1}$$

$$\nabla.\vec{J}_T = \nabla.\vec{J}_b + \nabla.\vec{J}_f \tag{2}$$

$$= -\frac{\partial \rho_b}{\partial t} - \frac{\partial \rho_f}{\partial t} \tag{3}$$

$$= -\frac{\partial}{\partial t}(-\nabla.\vec{P}) + \frac{\sigma.\rho_f}{\varepsilon} \tag{4}$$

$\vec{J}_b$ and $\vec{J}_f(=\sigma\vec{E})$ are the bound and free-current densities produced as a result of dielectric polarization $\vec{P}$ and the free-current density $\rho_f$ due to conductivity of the binder respectively. $\vec{E}$ is the electric field of the capacitor. $\sigma$ and $\varepsilon$ are the conductivity and permittivity of the binder respectively. The contribution of free-current density due to the presence of any mobile ions and loosely bound electrons within the dielectric is negligible when compared to that in the conductive binder.

The electric field due to a continuous volume charge distribution $\rho(\vec{r}')$ at $\vec{r}$ can be expressed as

$$\vec{E} = \frac{1}{4\pi\varepsilon_0}\int \rho(\vec{r}').\frac{\vec{r}-\vec{r}'}{\vec{r}-\vec{r}'^3}.d^3\vec{r}' \tag{5}$$

If a continuous charge distribution $\rho'(\vec{r})$ is present instead of a test charge 'q' at $\vec{r}$, then the force of interaction $\vec{F}'$ between $\rho(\vec{r}')$ and $\rho'(\vec{r})$ can be expressed as

$$\vec{F}' = \vec{E}.\int \rho'(\vec{r})d^3\vec{r} \tag{6}$$

In the case of a charged fibre bundle with a charge distribution $\rho'(\vec{r})$ on the bottom electrode of the capacitor, equation (6) can be expressed as

$$\vec{F}' = \vec{E}.\int \rho'(\vec{r})d^3\vec{r} = \frac{V}{d}\int \rho'(\vec{r})d^3\vec{r} \tag{7}$$

'V' and 'd' are the potential difference and the electrode separation respectively, with a uniform field 'V/d' in between. Therefore, the charge distribution of the fibre bundle determines the resulting motion. Due to inherent inhomogeneity in the binder distribution and the topography of the chopped end-faces of the fibre bundles, the charge distribution at the ends will be asymmetric. Therefore, the ends of the bundle will experience unequal forces ($F_1$ and $F_2$) of attraction towards the grounded electrode. The resulting torque induces rotation about the end with lower charge density until the bundle stands vertically on the bottom electrode. Subsequently, the bundle levitates vertically and adheres to the adhesive-backed cellulose paper on the grounded (top) electrode. The torque can be expressed as

$$\tau_N = (\delta Q_2 - \delta Q_1)\mathrm{EL}.\sin(\theta) \tag{8}$$

$\delta Q_1$ and $\delta Q_2$ are the fractional charges at either ends of the bundle of length L and $\theta$ is the angle between length L and $F_2$. Therefore, the bundle experiences rotation about the end with lower charge ($\delta Q_1$) until it is aligned along the field. As the bundle stands vertically with the $\delta Q_1$ end in contact with the bottom electrode, the force of attraction on the $\delta Q_2$ end increases according to the Coulomb's inverse square law, as it is closer to the top grounded electrode. In Figure 4, if the sum ($F_1$+$F_2$) acting along the same direction towards the top grounded electrode exceeds the weight 'mg' of the bundle, then it accelerates towards the top grounded electrode in a vertical fashion. Here, the effect of viscous drag in air is neglected as the frontal area of the bundle is small. The resultant of the forces on the bundle upon impact with the adhesive on the grounded electrode in conjunction with its

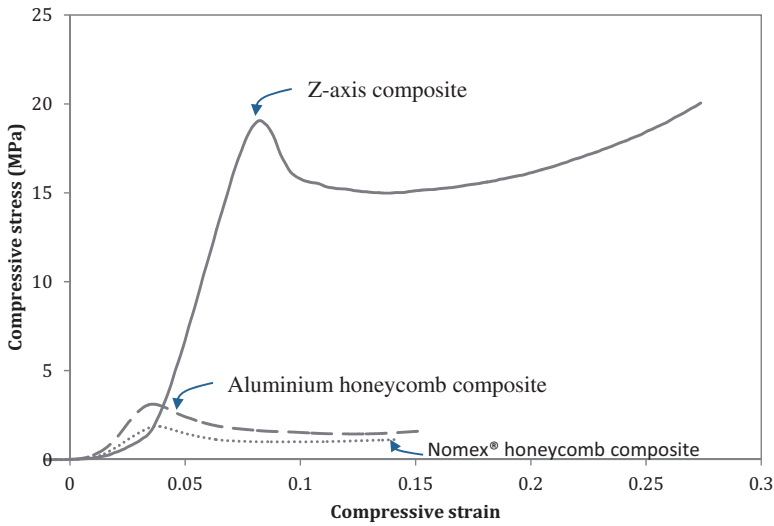


**Figure 5.** Typical stress/strain traces for the Z-axis, Nomex® and aluminium core sandwich composites.

topographical variations and mass distribution determine the orientation with respect to the electric field direction.

## *Comparison of mechanical properties*

***Flatwise compression:*** Typical compressive stress-strain traces for the aluminium and Nomex® honeycomb and the Z-axis composite sandwich panels are shown in Figure 5. The three samples displayed an initial non-linear region as the load was applied and transferred to the sandwich composites. This was followed by an elastic region for the three classes of composites where the load-bearing ability of the Z-axis composite is seen to be significantly superior when compared to the aluminium and Nomex® sandwich composites. The stress/strain behaviour of the Z-axis composite after the peak stress is also seen to be different when compared to the other two types of composites. In the case of the Z-axis composite, the peak compressive stress is followed by a decrease as the fibres fracture. This is then followed by compaction of the fracture fibres as the compression of the sandwich continues. The compressive loading of the aluminium and Nomex® sandwich composites were terminated before compaction was observed.

A summary of the flat-wise compressive strength for the Nomex® aluminium honeycomb sandwich and the Z-axis composites is presented in Figure 6. Batch-1 refers to the un-impregnated short-fibre Z-axis cores where the mean compressive strength was 1.04 MPa. The term un-impregnated refers to the case where the short-fibre arrays were not coated with the resin and cross-linked. The mean

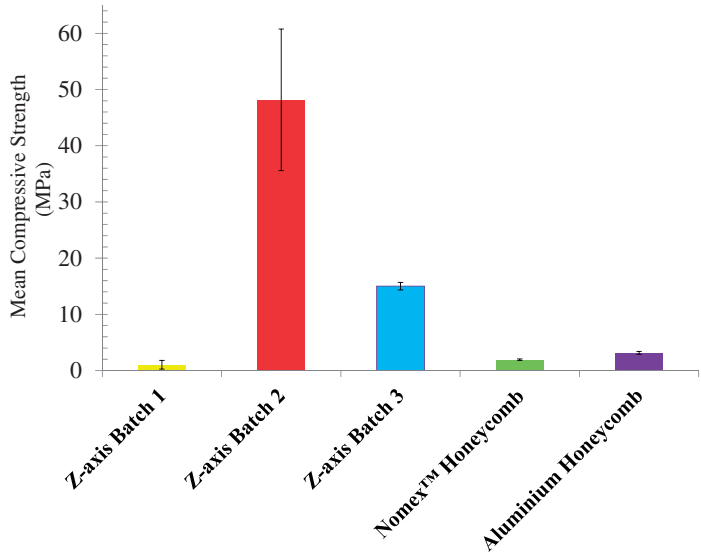


**Figure 6.** The mean compressive strengths of the 50×50 mm sandwich composites. Z-axis batches 1-3 correspond to un-impregnated, impregnated and controlled-mass samples where the total weights of the samples were equivalent to that of the Nomex® and aluminium honeycomb sandwich composites.

compressive strengths of the aluminium and Nomex® honeycomb sandwich panels were 3.15 and 1.91 MPa respectively. The compressive strengths stated by the manufacturer for the aluminium and Nomex® honeycombs are 3.93 MPa and 2.4 MPa respectively.

Figure 6 shows that the flatwise-compressive strength for Z-axis batch-2 (impregnated short-fibres and the matrix was cross-linked to produce the composite) is significantly superior to its conventional sandwich honeycomb counterparts. The average compressive strength of the Z-axis composite is 25.2 times that of Nomex® and 15.2 times that of aluminium. The average mass of the Z-axis batch-2 samples was only 1.31 and 1.28 times heavier than the equivalent Nomex® and aluminium honeycomb sandwich composites respectively.

On inspecting Figure 6, it is apparent that Z-axis batch-2 composites exhibit a relatively large variation in the compressive strengths. This is despite the fact that the total weight of the short-fibre bundles in the core was controlled for batch-2. This scatter in the flat-wise compressive strength observed in the Z-axis data may be attributed to one or more of the following factors:

(i) The variation in resin content between the samples. The mode of impregnation used in the current study relied on capillary action. Although the binder

content in the short-E-glass fibre bundles was not determined, previous studies have shown that it can be variable. Hence, the impregnation efficiency may not have been uniform. The degree of impregnation is important as the matrix not only enables the creation of vertically-aligned beams of Z-axis preforms but it also provides significant lateral confinement and restraint for the short-fibre when subjected to compressive loading.

(ii) In this proof-of-concept study, the binder system on the short-E-glass fibres used in this study was formulated for thermoplastic-resins. Therefore, the interfacial bond strength between the fibres and the matrix was not ideal. Nevertheless, it was sufficient to demonstrate the Z-axis sandwich composite concept.

With reference to the average mass of the Z-axis batch-2 samples mentioned previously, in weight-critical applications, this increased weight may not be a favourable proposition. Therefore, further Z-axis composite samples were manufactured and coded as batch-3. In these samples, the primary aim was to match their weights to that of the Nomex® and aluminium sandwich composites. These lighter Z-axis composites displayed lower compressive properties when compared to batch-2 primarily due to the reduced fibre and resin contents. However, compressive strengths were still significantly higher than the Nomex® and aluminium honeycomb core samples. The standard deviations for batches-2 and 3 were 12.6 MPa and 2.3 MPa respectively. This suggests that the Z-axis fibre content, orientation and impregnation efficiency has a major influence on the flatwise compressive strength and controls the consistency of the Z-axis composite.

Figure 7 illustrates the flatwise compressive stiffness for the different types of sandwich composites manufactured in this study. As expected, the un-impregnated

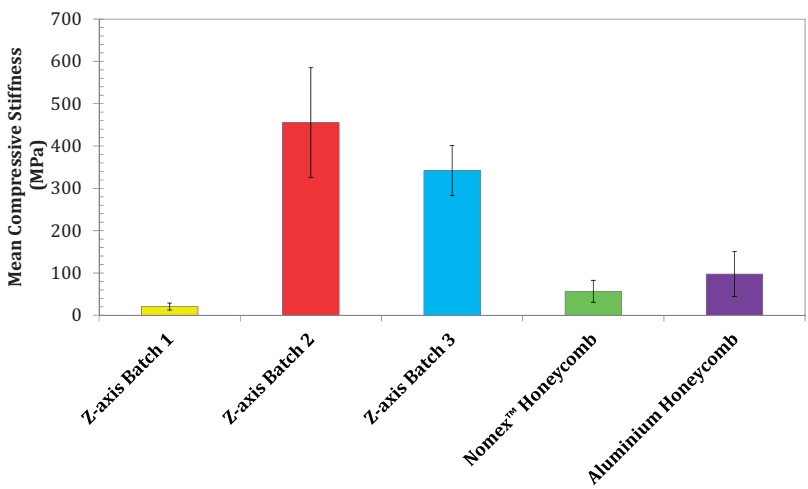


**Figure 7.** The mean compressive stiffness of Z-axis and honeycomb sandwich panels.

samples (batch-1) had poor compressive stiffness when compared to the other sandwich composites. However, as seen in Figure 7, batches-2 and 3 exhibit improved compressive stiffness when compared to the Nomex® and aluminium core sandwich composites. The batch-3 samples had a mean compressive stiffness that is 8.03 and 4.67 times greater than the Nomex® and aluminium core sandwich composites respectively.

As mentioned previously and with reference to Figure 6, the scatter in compressive strength for batch-3 was reduced when compared to batch-2 when the resin content was controlled. In order to investigate this further, additional Z-axis composite samples were fabricated where the fibre content was maintained constant but the weight of the resin was varied. Figure 8(a) shows the relationship between resin content and the compressive strength for the Z-axis composites where a good correlation is observed between the two parameters. A similar trend is observed for the compressive stiffness as a function of the resin content illustrated in Figure 8 (b). Visual inspection of the samples indicated that three factors may have been responsible for the trend in the data. Firstly, when the resin content was intentionally low, it was observed that the bonding between the vertically-aligned fibre bundles and the composite skins was not consistent and some resin depleted areas were observed. Visual evidence for this is presented in Figure 9(a) to (d). In Figure 9(a) a minute gap was seen between the bottom composite skin and the end of the vertically-aligned fibre. As the compressive load was applied (Figure 9 (b)), the fibre was still unloaded. It made contact with bottom composite skin after an applied strain of 0.4 (see Figure 9(c) and (d))

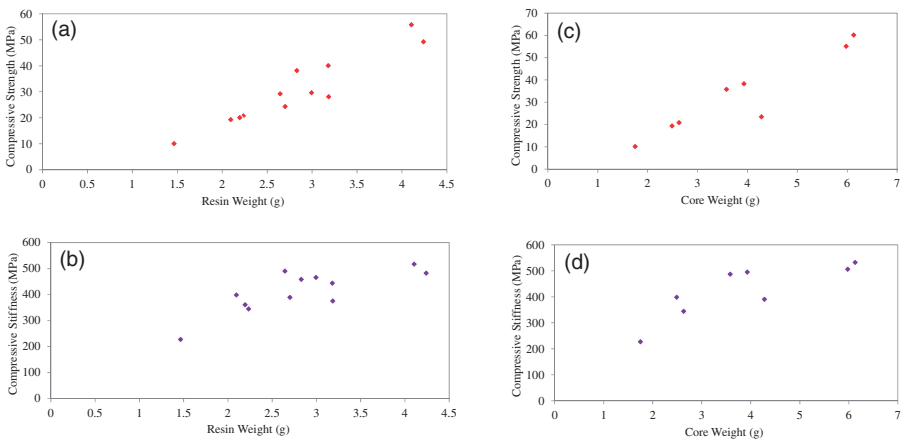


**Figure 8.** Effect of the resin and fibre core content on the compressive strength and stiffness: (a) compressive strength versus resin content; (b) compressive stiffness versus resin content; (c) compressive strength versus the weight of the Z-axis fibres in the core; and (d) compressive stiffness versus the weight of the Z-axis fibres in the core.

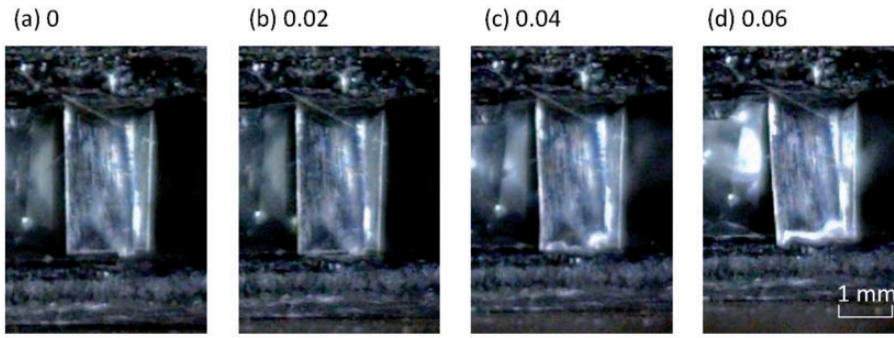


**Figure 9.** (a to d) Real-time imaging of a single-fibre bundle within a Z-axis composite, during compression testing where the resin content was made intentionally low. The numbers on the top of each image corresponds to the compressive strain on the sample when each image was acquired. A minute gap can be seen at zero strain where the fibre bundle is not in contact with the bottom skin. Contact between the fibre bundle and the composite skin is made at an applied strain of 0.04.

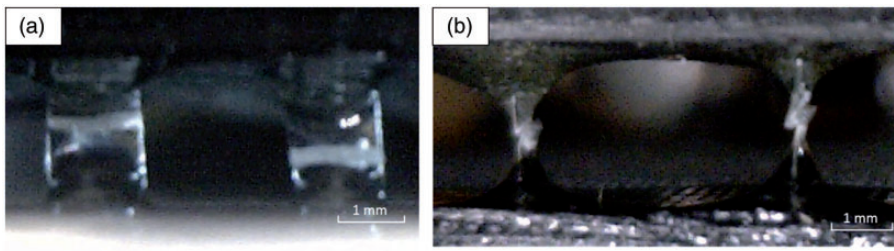


**Figure 10.** (a) Front view image of kink bands normal to the fibre direction forming in fibre bundles in the reference sample. (b) Side view image of fibre bundle fracture in the reference sample, following the formation of kink bands normal to the fibre direction.

Secondly, in the samples where the resin content was intentionally low, as expected, sections of un-impregnated fibres were observed. Thirdly, in the composites with a low resin content in the core, a significant proportion of the fibre bundles buckled during compressive loading. However, in the samples with a higher resin content, where the impregnation was complete, fibres failed predominantly by fracture. Previous researchers have also proposed that the resin can act as a support against buckling. For example, polymer foams were reported to increase the buckling strength of Z-pins [5,6]. X-cores with thicker columns tended to fracture whilst thinner ones buckled elastically [10] and the same conclusion was reached when using corrugated cores [13].

The fracture behaviour of the fibres was investigated further by manufacturing a "reference" Z-axis composite where each Z-axis E-glass fibre bundle was bonded and impregnated manually. The previously mentioned imaging system was used to record

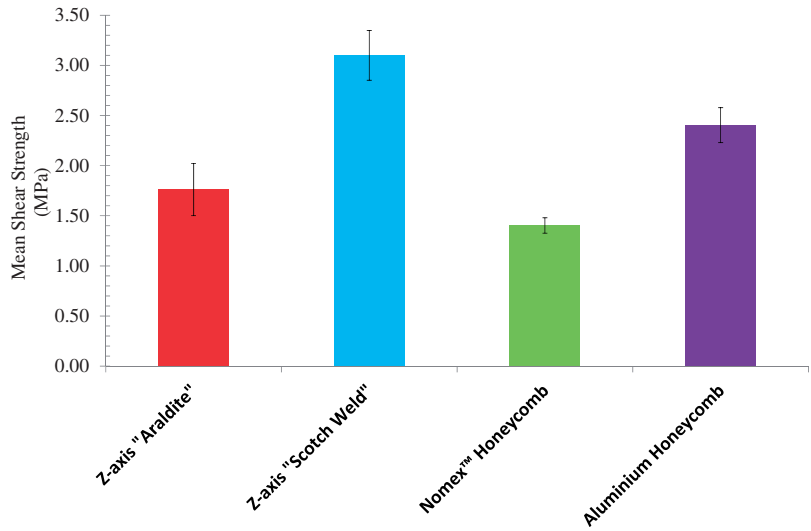


**Figure 11.** Comparison of the sandwich composite shear strengths with specified core materials.

the compressive loading of the fibres in real-time. With reference to Figure 10, kink bands were seen to form normal to the fibre direction prior to fracture. It can be concluded that when all fibres are impregnated completely, with adequate resin at the boundary between the skin and Z-axis fibres, the predominant mode of failure is via compressive fracture induced by the formation of kink bands as opposed to buckling. In other words, it is proposed that each of the Z-axis fibres acts as a vertically-aligned composite beam.

Following the examination of the effect of the weight of the resin content in the core on compressive strength, a further set of Z-axis composites were manufactured to investigate the effect of varying the weight of the fibre bundles (core). Figure 8(c) and (d) shows a positive correlation between the fibre content in the core and the compressive strength and stiffness respectively.

***Shear strength and stiffness:*** The data for the mean shear strength and stiffness for the Z-axis and conventional honeycomb composites are presented in Figures 11 and 12 respectively. It is apparent that the Z-axis sandwich composite exhibited higher shear strength and stiffness when compared to the Nomex® core material but not the aluminium. In this current proof-of-concept study, the Rapid-Araldite resin system was used as it was convenient. In order to demonstrate that the shear properties of the Z-axis composites can be improved, six further Z-axis composites were manufactured using an alternative resin for bonding the short-fibre preforms to the skins. In this instance, the skins were bonded to the Z-axis preform with Scotch-Weld 9323, prior to impregnation. This adhesive was selected due to its higher lap-shear strength (3M, 2013) than Araldite-Rapid. As seen in Figures 11

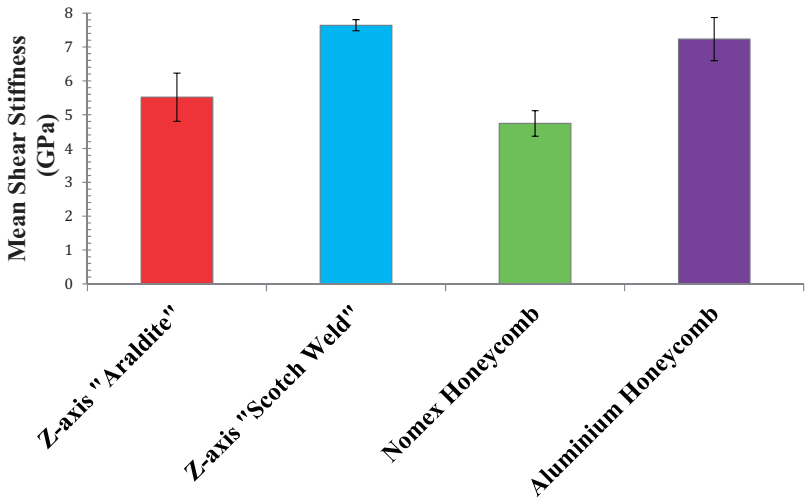


**Figure 12.** Comparison of the sandwich composite shear stiffnesses with specified core materials.

**Table 1.** Summary of the mean flexural strength, transverse shear rigidity and core shear modulus for the Nomex® and aluminium honeycomb, and Z-axis composites.

| Material/property | Nomex™ honeycomb | Aluminium honeycomb | Z-axis composite |
|---|---|---|---|
| Mean flexural strength ($MNmm^2$) | 53.4 (9.8) | 105.9 (43.1) | 87.6 (63.2) |
| Mean transverse shear rigidity (kN) | 30.2 (8.4) | 45.9 (10.7) | 37.1 (18.0) |
| Mean core shear modulus (MPa) | 0.065 (0.018) | 0.097 (0.023) | 0.079 (0.038) |

and 12, the mean shear strength and stiffness respectively of the Scotch-Weld resin-bonded Z-axis samples was higher than their honeycomb counterparts.

***Flexural strength, transverse shear rigidity and shear modulus:*** A summary of the mean flexural strength, transverse shear rigidity and shear modulus is presented in Table 1. The numbers in parenthesis represents the standard deviation for each class of material. With reference to Table 1, it is apparent that the above-mentioned properties of the Z-axis composites are in between that of the Nomex® and aluminium honeycomb sandwich composites. It is also clear that the scatter in the data for the Z-axis composites is significantly higher. The primary reasons for the observed scatter are: (i) in these specimens, the core was bonded to the skins using the LY3505/XB3403 resin and hardener; and (ii) due to the length of the test specimen, the Z-axis core was manufactured in two sections and assembled to produce the flexural test specimens. It is proposed that optimising the production methods for the shear and flexural test specimens in tandem with the

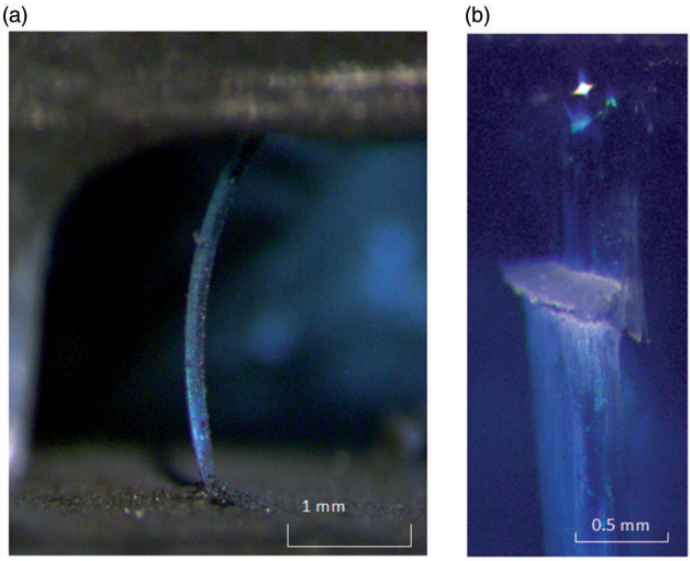


**Figure 13.** Micrograph of a 3 mm long E-glass fibre bundle composite undergoing: (a) buckling; and (b) fracture subsequent to the formation of a kink band.

deployment of resins with high-shear strength will enable the core-skin bond strength to be improved.

## *General failure modes*

The dominant failure modes observed with the Z-axis composites when they were subjected to flatwise compression were Euler buckling and kink band-induced fracture of the vertically-aligned short-E-glass fibres. Figure 13(a) and (b) shows examples of E-glass fibre bundles in the Z-axis sandwich undergoing buckling and fracture via a kink band formation respectively. Figure 14 illustrates sequential micrographs that were recorded as a function of time during a flatwise compression test. The formation of an inclined kink band in the E-glass fibre bundle within the Z-axis composite is readily apparent. The aluminium and Nomex® honeycomb sandwich composites failed by buckling of the cell walls; the failure mode for a Nomex® sandwich sample during flatwise compression is shown in Figure 15. With reference to the flexural samples, in the case of the Nomex® sandwich composites, failure occurred through collapse of the honeycomb cell walls. The aluminium core sandwich panels however experienced cracking of the skin along with localised crushing of the core. The Z-axis samples failed abruptly through the de-bonding of the skin and core. Similar failure modes were reported in the literature [5,40]. For example, in composite sandwich panels where struts were present in some form

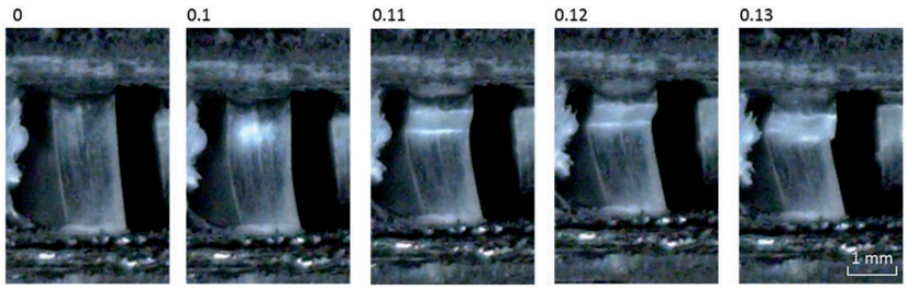


**Figure 14.** Real-time imaging of the formation of an inclined kink band in an E-glass fibre bundle within a Z-axis composite. All images represent the same fibre bundle but at different stages of the loading process. The values above each image refer to the compressive strain experienced by the sample at the time the image was taken.

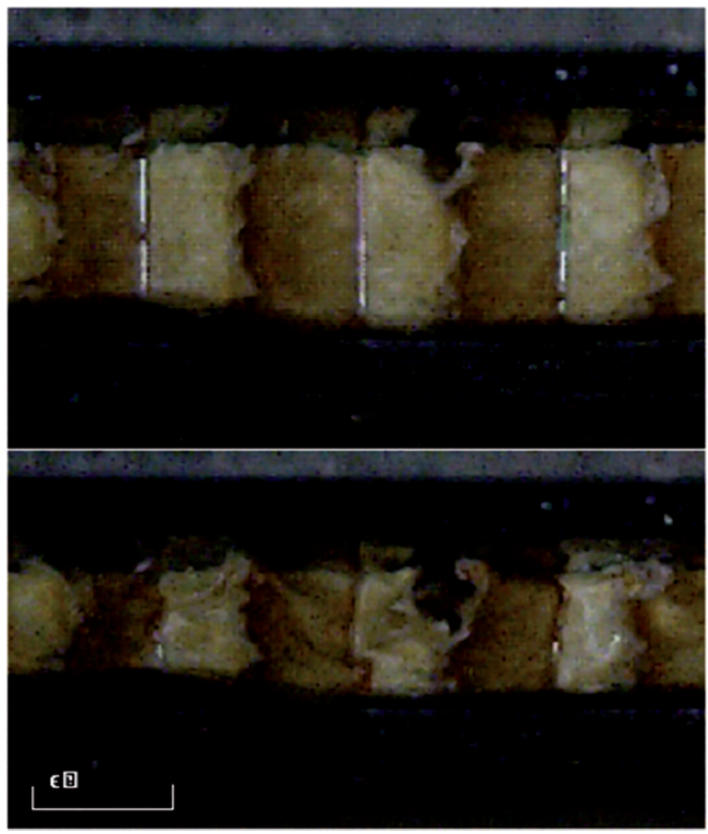

**Figure 15.** Side-view image of a Nomex® honeycomb sample (top) prior to and (bottom) following loading. Shear bands can be seen in the bottom image where the walls of the honeycomb have buckled.

(elongated Z-pins in X-cores, columns formed around stitches, or trusses) failure at the core-skin interface was observed commonly.

### Models on compressive loading of unidirectional and sandwich composites

A general review on the strength and stiffness of short-fibre, and sandwich composites can be found in references [41] and [42] respectively. Finite element modelling of Z-pinned fibres include the works of Grassi et al. [43] and Meo et al. [44]. It is proposed that the theories that are used to predict the properties of short-fibres [45] and Z-pinned composites [6,46,47] can be adapted and used with the current Z-axis composites. The micromechanics for the Z-axis composite is presented in Appendix-A.

### Prospects for scaling up the production of Z-axis composites

When contemplating the scaling up of the Z-axis manufacturing process, a number of issues have to be considered including the following.

(i) Adhesive-backed cellulose paper: In the laboratory study, this method was chosen for convenience. The adhesive had the appropriate tack to secure the spatial orientation of the vertically-aligned short-fibre preforms. Moreover, it was sufficiently thin for the applied electric field to be not impaired significantly with regard to the grounded electrode. Other classes of non-conducting and flexible materials such as polymers and resin films can also be used. In contemplating a continuous production process involving a conveyor belt-based system, the adhesive-backed cellulose paper (similar in dimensions to that used in the prepreg or printing industries) can be fed and maintained in intimate contact to the grounded electrode. In some circumstance, the carbon fibre skin itself can be used as the grounded electrode and the short-fibres can be deposited directly on to it, secured and impregnated.

(ii) Securing the spatial orientation of the vertically-aligned short-fibre preform: A number of adhesives can be used to achieve this objective. For example, photo-curing resins can be used because light can be coupled through the end-face of the E-glass fibres [48]. Resin films that are used conventionally to bond honeycombs to the skins can also be used. Moreover, the same resin system that is used to impregnate the vertically-aligned short-fibres can be sprayed on before the short-fibres are deposited. As the production process is intended to be continuous, localised heating, can be used to partially cross-link the adhesive. A number of resin suppliers offer hardener formulations to achieve specified rates of cross linking; this applies to the LY3505/XB3403 resin system used in the current study. Provided the cost and the desired properties for the Z-axis composites are not compromised, it was shown in Figure 11 that the resin system that is used to bond the vertically-aligned fibre

can be deployed to optimise the mechanical properties. It is worth noting that the orientation of the short-fibres can be inclined at any desired angle after the fibres are deposited on the substrate and before the resin is partially cross-linked. In such a scenario and if the adhesive-backed substrate is flexible, the short-fibre arrays can be draped over complex shapes or used to produce horizontally-aligned short-fibre preforms and prepregs.

(iii) Length of the short-fibres: In practice, applications will dictate the need for cores of different thicknesses. A similar procedure to that described here can be used to manufacture Z-axis composites using the current range of commercially available (up to 14 mm) "uniaxial" short-fibres. The issue with producing longer chopped fibres from conventional creels or bobbins is the intrinsic curvature in the continuous fibres. The radius of curvature will vary when traversing from the bore to the outer surface of the creel [39]. If longer uniaxial short-fibres are required, the production will have to be modified to eliminate the intrinsic curvature before the fibres are chopped. This can be achieved by extracting the fibres from the outer circumference or bore (if intermittent twists can be tolerated) using a pinch-roller payout system. The fibre bundles will have to be impregnated or wetted with a non-toxic low-boiling point solvent or the original binder solution and dried under tension; this will remove the original crimp and curvature present on the fibre. The fibres can be chopped using conventional methods. Another possible method to produce longer uniaxial short-fibres is to contemplate pultrusion where a large array of uniaxial short-fibres can be produced in the form of rectangular strips or circular rods. Another viable technique is to stack the core and this was proposed previously [21]. This approach will provide options for the development of unique hybrid cores.

(iv) Controlling the fibre volume fraction in the core: In the current study, the grounded electrode with the cellulose paper and the vertically-aligned short-fibres were removed from the rig and weighed periodically to determine weight of the reinforcement. Obviously, this will not be practical in any continuous production method. Image analysis has been used previously to detect the fracture of individual filaments in a composite [48]. A similar approach can be adapted to detect the perimeter of the ends of the short-fibres as they are deposited on the grounded electrode. Alternatively, a calibration curve can be generated to quantify the deposition rate of the short-fibres as a function of time for a given set of operating and environmental conditions. A low-cost option would be to use an instrumented conveyor belt to determine the removal and/or deposition of the short-fibre.

(v) Controlling the location where the short-fibres are deposited: In cases where there is a need to distribute the short-fibres to predefined regions, this can be achieved by using a patterned grounded electrode or by having segmented grounded electrodes where each one is activated using a computer-controlled switching unit.

(vi) Impregnating the vertically-aligned short fibre: This can be carried out in a number of ways. For example, the dip-coat method used in this study could be implemented. The excess resin can be removed by bringing it into contact with an absorbent material. However, this will contribute to the consumables cost and generate waste. One option is to spray the resin in a controlled manner to impregnate the short-fibres where the required quantity of the resin is delivered.

(vii) Production cost: This aspect requires a detailed cost analysis but a rough comparison can be made with the conventional Nomex honeycomb. The cost of an equivalent short-E-glass fibres is £1.35/kg. The LY3505 resin and XB3403 hardener costs £9.15 and £14.87 per kg respectively. In the current study, in one set of controlled samples (where the weights of the core and resin used were quantified), 0.33 g of short-fibres and between 1.47 and 4.24 g of the resin system (mixed resin and hardener) were used to produce a preform of dimensions 50 x 50 mm. Assuming a weight of 2.85 g for the resin system (accounting for over-impregnation), scaling this up, 1 kg of the short-fibres can be used to produce approximately ten preforms of dimensions 1 $m^2$. The current cost of purchasing Nomex® honeycomb with a 3.2 mm cell with a thickness of 3 mm is £27.30 for a dimension of 600 x 600 mm.

### *Other potential applications for the Z-axis composite*

The Z-axis technology reported here can be adapted for a wide range of designs and applications. For example, the E-glass fibres can be replaced with carbon fibres in order to improve the specific properties further. E-glass can also be substituted with short-alumina and sapphire fibres for high-temperature application where the skins and resins are replaced with materials that can sustain significantly higher melting/degradation temperatures when compared with their organic counterparts. The vertically-aligned fibres do not necessarily have to be rods or rectangular plates, they can be composite coils and these can be used as cores in the form of springs. In the Z-axis composite design, the space between the vertically-aligned fibres can be used as cooling/heating channels with an appropriate fluid being permitted to flow through. There are realistic options for "smart" composites to be manufactured where for example, two or more short-fibre lengths can be used where the longer ones are used for bonding to the skins and the other for applications such as energy harvesting, vibration damping and damage detection. The prospect for optical data and image transmission/projection are realistic prospects as it is known that E-glass can transmit light [48]. Here, the skins and resins will have be chosen such that they are transparent to the wavelength of interest. It is anticipated that on the basis of the superior flat-wise compressive properties of the Z-axis composites, their impact properties can be engineered by selecting different or hybrid fibres and low-density matrices. Filling the spaces in between the short-fibres with an energy absorbing material such as Surlyn™ will

be of interest as it will provide additional restraint to the vertically-aligned short-fibres and it is known to have self-healing characteristics [49].

## Conclusions

The Z-axis composites exhibited out-of-plane compressive strengths that were over an order of magnitude higher than equivalent sandwich panels made with Nomex® and aluminium honeycomb cores [50]. The shear strength and stiffness of these Z-axis composites was also found to be superior to the honeycomb sandwich panels. Although the production of the Z-axis flexural specimens was not optimised, the flexural strength was higher than that of the Nomex® core sandwich composites but lower than that of the aluminium sandwich composite.

In situations where a high out-of-plane compressive strength is desired, it may be particularly advantageous to select a Z-axis composite over an alternative sandwich panel. The resistance to out-of-plane compression is provided without a significant reduction in the in-plane properties. It was found that the number of fibre bundles within the core of a Z-axis composite correlated positively with the out-of-plane compressive properties. This offers the opportunity to tailor the electrostatic manufacturing process to vary the final properties of the sandwich panel. For example, it allows control over the number of fibre bundles that are deposited to form the core. Furthermore, if a particular section of a sandwich panel requires increased out-of-plane compressive strength or stiffness, there is potential for the density of fibre bundles in that section to be increased accordingly.

### Acknowledgments

Robbie White (MSc) acknowledges funding from the Engineering and Physical Sciences Funding Council. Mark Paget and Gerard Fernando wish to thank Dr Garry Wells and the MoD/DSTL for MAST funding for the Z-axis demonstrator study. Ashwini Prasad will like to acknowledge funding from Innovate UK (Project AB135A). The authors are grateful to Professor Brian Ralph, Dr JDR Talbot, Frank Biddlestone, Carl Meggs and Jeremy Ahern for technical comments and assistance.

### Declaration of Conflicting Interests

The author(s) declared no potential conflicts of interest with respect to the research, authorship, and/or publication of this article.

### Funding

The author(s) disclosed receipt of the following financial support for the research, authorship, and/or publication of this article: This work was supported by Ministry of Defence (DSTL/MAST), Engineering and Physical Sciences Research Council (MSc Studentship (R White)), and Innovate UK (Project AB135A).

### ORCID iD

Gerard F Fernando https://orcid.org/0000-0003-2524-5170

## Supplemental Material

Supplemental material for this article is available online.

## References


1. Paik JK, Thayamballi AK and Kim GS. The strength characteristics of aluminum honeycomb sandwich panels. *Thin Wall Struct* 1999; 35: 205–231.
2. Zhang J and Ashby M. The out of plane properties of honeycombs. *Int J Mech Sci* 1992; 34: 475–489.
3. Sypeck DJ. Cellular truss core sandwich structures. *Appl Compos Mater* 2005; 12: 229–246.
4. Cote F, Russel BP, Deshpande VS, et al. The through-thickness compressive strength of a composite sandwich panel with a hierarchical square honeycomb sandwich core. *J Appl Mech* 2009; 76: 061004.
5. Marasco AI, Cartie DDR, Partridge IK, et al. Mechanical properties balance in novel z-pinned sandwich panels: out of plane properties. *Compos Part A Appl S* 2006; 37: 295–302.
6. Cartie DD and Fleck NA. The effect of pin reinforcement upon the through thickness compressive strength of foam-cored sandwich panels. *Compos Sci Technol* 2003; 63: 2401–2409.
7. Steeves CA and Fleck NA. In-plane properties of composite laminates with through-thickness pin reinforcement. *Int J Solids Struct* 2006; 43: 3197–3212.
8. Tong L, Mouritz AP and Bannister MK. Manufacture of 3D fibre preforms. In: *3D fibre reinforced polymer composites*. Kidlington: Elsevier, 2002. Chapter 8 - Stitched Composites: 163-204.
9. Wang B, Wu L, Jin X, et al. Experimental investigation of 3D sandwich structure with core reinforced by composite columns. *Mater Des* 2010; 31: 158–165.
10. Malcom AJ, Aronson MT, Deshpande VS, et al. Compressive response of glass fiber composite sandwich structures. *Compos Part A Appl S* 2013; 54: 88–97.
11. He L, Cheng Y and Liu J. Precise bending stress analysis of corrugated-core, honeycomb-core and X-core sandwich panels. *Compos Struct* 2012; 94: 1656–1668.
12. Mouritz AP, Leong KH and Herszberg I. A review of the effect of stitching on the in-plane mechanical properties of fibre-reinforced polymer composites. *Compos Part A Appl S* 1997; 28: 979–991.
13. Xiong J, Ma L, Pan S, et al. Shear and bending performance of carbon fiber composite sandwich panels with pyramidal truss cores. *Acta Mater* 2012; 60: 1455–1466.
14. Zhang G, Ma L, Wang B, et al. Mechanical behaviour of CFRP sandwich structures with tetrahedral lattice truss cores. *Compos Part B Eng* 2012; 43: 471–476.
15. Mitra N. A methodology for improving shear performance of marine grade sandwich composites: sandwich composite panel with shear key. *Compos Struct* 2010; 92: 1065–1072.
16. Cinar K. Evaluation of sandwich panels with composite tube-reinforced foam core under bending and flatwise compression. *J Sandw Struct Mater* 2020; 22: 480–493.
17. Zhou J, Guan ZW, Cantwell WJ, et al. The energy-absorbing behaviour of foam cores reinforced with composite rods. *Compos Struct* 2014; 116: 346–356.
18. Abdi B, Azwan S, Abdullah MR, et al. Flatwise compression and flexural behaviour of foam core and polymer pin-reinforced foam core composite sandwich panels. *Int J Mech Sci* 2014; 88: 138–144.

19. Balikoglu F, Demircioglu TK, Yildiz M, et al. Mechanical performance of marine sandwich composites subjected to flatwise compression and flexural loading: Effect of resin pins.. *J Sandw Struct Mater* 2020; 22: 2030–2048.
20. Eyvazian A, Moeinfard M, Musharavati F, et al. Mechanical behaviour of resin pin-reinforced composite sandwich panels under a quasi-static indentation and three-point bending loading conditions. *J Sandw Struct Mater*. Epub ahead of print 2020. DOI: 10.1177/1099636220909752.
21. Yalkin HE, Icten BM and Alpyildiz T. Tensile and compressive performances of foam core sandwich composites with various core modifications. *J Sandw Struct Mater* 2017; 19: 49–65.
22. Fernando GF. Energy Efficient and Environmentally Friendly Recycling of Composites. TSB Final Report. Innovate UK Project Number 100533 (AB135 A). 2011.
23. Prasad A. Application of electrostatics to align short-glass fibre bundles for composite manufacturing. MPhil Thesis. University of Birmingham. 2012. http://etheses.bham.ac.uk/id/eprint/4363
24. Degamber B and Fernando GF. Fibre optic dilato-spectroscopic sensor: simultaneous thermal, spectral, and physical analyses of materials. *Smart Mater Struct* 2006; 15: 1054–1062.
25. Pandita SD, Irfan MS, Machavaram VR, et al. Clean wet-filament winding–part 1: design concept and simulations. *J Compos Mater* 2013; 47: 379–390.
26. Mahendran RS, Wang L, Machavaram VR, et al. Fiber-optic sensor design for chemical process and environmental monitoring. *Optics Lasers Eng* 2009; 47: 1069–1076.
27. Machavaram VR, Wang L, Pandita SD, et al. Multi-point monitoring of cross-linking reactions. *J Appl Polym Sci* 2014; 131: 41088.
28. Carbon fibre skins: VTM® - Product catalogue | Solvay
29. Short-E-glass fibres: HP3540_200714.pdf (neg.co.jp)
30. Scotch-Weld adhesive: AAMD Technical Data Sheets (3m.com)
31. Thermosetting resin for impregnation of the short-fibres: Araldite LY 3505_Hardener XB 3403_XB 3404-1_Aradur 3405_eur_e.doc (swiss-composite.ch)
32. ASTM, C393/393M, Standard test method for core shear properties of sandwich construction by beam flexure, 2011.
33. ASTM, C365/C365M, Standard test method for flatwise compressive properties of sandwich cores, 2011.
34. ASTM, C273/C273M, Standard test method for shear properties of sandwich core materials, 2011.
35. ASTM D7250/D7250M, Standard practice for determining sandwich beam flexural and shear stiffness, 2006.
36. Properties of E-glass fibres: Properties: E-Glass Fibre (azom.com)
37. Pionteck J and Wypych G. *Handbook of antistatics*. 2nd ed. Scarborough: Chem Tech Publishing, 2017.
38. Griffiths DJ. *Introduction to electrodynamics*. 4th ed. London: Pearson Publishing, 2012.
39. Irfan MS, Machavaram VR, Mahendran RS, et al. Lateral spreading of a fiber bundle via mechanical means. *J Compos Mater* 2012; 46: 311–330.
40. Lascoup B, Aboura Z, Khellil Z, et al. On the mechanical effect of stitch addition in sandwich panel. *Compos Sci Technol* 2006; 66: 1385–1398.
41. Fu SY, Lauke BL and Mai YW. *Science and engineering of short fibre reinforced polymer composites*. Cambridge: Woodhead Publishing, 2009.

42. Hu H, Belouettar S, Potier-Ferry M, et al. Review and assessment of various theories for modelling sandwich composites. *Compos Struct* 2008: 84: 282–292.
43. Grassi M, Zhang X and Meo M. Prediction of stiffness and stresses in z-fibre reinforced composite laminates. *Compos Part A* 2002; 33: 1635–1664.
44. Meo M, Achard F and Grassi M. Finite element modelling of bridging micro-mechanics in through-thickness reinforced composite laminates. *Compos Struct* 2005; 71: 383–387.
45. Halpin JC. Stiffness and expansion estimates for oriented short fiber composites. *J Compos Mater* 1969; 3: 732–734.
46. Mouritz AP. Compression properties of z-pinned sandwich composites. *J Mater Sci* 2006; 41: 5771–5774.
47. Nanayakkara A, Feih S and Mouritz AP. Experimental analysis of the through-thickness compression properties of z-pinned sandwich composites. *Compos Part A* 2011; 42: 1673–1680.
48. Malik SA, Wang L, Curtis PT, et al. Self-sensing composites: in-situ detection of fibre fracture. *Sensors* 2016; 16: 615.
49. Harris D, Mahendran RS, Brooks D, et al. Self-sensing, self-healing, and crack-arrestor composites. Proceedings Volume 7293, Smart Sensor Phenomena, Technology, Networks, and Systems 2009; 72930P (2009). SPIE Smart Structures and Materials + Non-destructive Evaluation and Health Monitoring, 2009, San Diego, California, United States. https://doi.org/10.1117/12.817617
50. Fernando G, Paget M. Composite sheet material.US Patent Application Number 1708829.5. 2019.